Nanopore functionalized by highly charged hydrogels for osmotic energy harvesting

Tianji Ma, Emmanuel Balanzat, Jean-Marc Janot, Sébastien Balme

Nanopore Functionalized By Highly Charged Hydrogels For Osmotic Energy Harvesting

*Tianji Ma[1], Emmanuel Balanzat[2], Jean-Marc Janot[1], Sébastien Balme[1]**

[1]Institut Européen des Membranes, UMR5635 UM ENSM CNRS, Place Eugène Bataillon, 34095 Montpellier cedex 5, France

[2]Centre de recherche sur les Ions, les Matériaux et la Photonique, UMR6252 CEA-CNRS-ENSICAEN, 6 Boulevard du Maréchal Juin, 14050 Caen Cedex 4, France.

*To whom correspondence should be addressed sebastien.balme@umontpellier.fr.

Keywords: Nanopore, osmotic energy, current rectification, polyacrylamide gel

Abstract: The salinity gradient between brine and fresh water is an abundant source of power which can be harvested by two major membrane methods: pressure-retarded osmosis and reversed electro-dialysis. Nowadays, the latter technology is close to real application but still suffer from low power yield. The low membrane selectivity as well as complex membrane fabrication are main limiting factors. To improve that, we design a couple of ion selective membranes based on track etched polymer nanopore functionalized by highly charged hydrogels. Two nanopore geometries are compared to present a preferential of cylindrical shape than conical shape that have a good ability of generating osmotic energy with gel functions and more importantly can be scaled up. Experiments from single nanopore, multipore membrane to stacked membranes shows a complete characterization from ionic transportation to energy generation and a clear relationship from single pore to stacked membranes. In the actual experiment conditions, it achieved a power density of 0.37 W m^{-2} at pH 7. By improving ionic tracks and reducing inter membrane distances; it can be a good candidate for industrial applications.

1. Introduction:

Energy and environment are currently two of the main topics for modern society thanks to the global warming. Until today, fossil fuels are used as the primary energy source to support human life and also generate both environmental and ecological problems[1–3]. Although, a variety of sustainable energy sources are being exploited such as biofuel[4], solar[5], wind[6], geothermal electricity[7] and water[8]. In this context, the osmotic energy (called also blue energy) which takes advantage of the salinity difference between sea water and river water could be a good candidate thanks to the renewability of the resource, the pollution free, relatively low cost and rich

reserves[9]. The estimated production of blue energy is closed to 2 TW which can fulfill the electricity demand today[10].

To practically make use of this large energy from water, the efforts were made to develop two methods based on membrane separation processes[11]: pressure retarded osmosis (PRO) and reversed electro-dialysis (RED). For the PRO facilities, a semipermeable membrane is placed between river water (feed solution with low osmotic pressure) and sea water (draw solution with high osmotic pressure). Water pass from feed to draw solution driven by the osmotic pressure difference[12,13]. By equipping a turbine to the reservoirs of draw solution, the energy of this water flow is converted to electricity. In RED technology, stacked ion exchange membranes (IEMs) are used. The ions move selectively from concentrated salt solution to diluted one driven by salinity gradient[14,15]. The charge flow of the ion separation is converted into electric current by redox reaction of electrodes. The energy harvested by this technology is relatively low and to make it suitable for real application an effort is essential to improve the performance of membranes.

To develop both anion exchange membranes and cation exchange membranes, many materials were used to improve the power density, the energy efficiency and the cost of membranes[8,16]. Recently the investigation at single nanopore level has allowed major fundamental breakthrough for further application. Indeed, Siria, A. et al. measured giant osmotic energy through a single boron nitride nanotube with a diameter between 100 nm and 200 nm, providing a power generation of 20 pW pore^{-1} (C_{max}/C_{min} = 1000)[17]. Feng, J. et al. synthesized a single sheet of MoS_2 nanopore with a diameter of 5 nm and a membrane thickness of only 0.65 nm. This single sheet structure generates an osmotic current at more than 8 nA and a single pore power at almost 0.5 nW (C_{max}/C_{min} = 1000)[18]. Despite impressive result at single pore scale, these nanopores

cannot be scaled up on large area of multipore membranes for practical uses by now. Besides of these, 2D materials based on graphene oxides have also been considered for RED application J. Ji et al. utilized a negative/positive charge graphene oxide membrane to get a power density of 0.77 W m^{-2} [19]. As nanotube, these 2D materials are particularly efficient since they combine both surface charge and/or large slippage to generate osmotic energy[9,20]. Beside the surface charge, the asymmetrical structure of nanopore generates also the ionic selectivity[21–23]. Recently, L. Jiang's group has developed a package of asymmetrical heterogeneous membranes which take advantage of both charge and membrane asymmetry. They used mesoporous carbon/macroporous alumina membrane[24] to achieve a power density at 3.46 W cm^{-2}. Two block copolymers[25] are synthesized to get a power density of 2.04 W cm^{-2}.is from combining porous block copolymer with track-etched PET membrane a power density of 0.35 W cm^{-2} was reached [26]. While they suffer from fragility of alumina support, complexity of fabricating composite membranes or the low pore density of conical nanopore.

In this work, we want to tackle the main issue related to conical nanopore obtained by track-etched method to propose a membrane stack with high nanopore density taking the advantage to a polymer support. Indeed the fabrication and physical-chemistry properties of such membranes have been well exploited[27–31]. It is thus possible to play with both asymmetrical geometry and surface charges to develop an ionic diode like ion exchange membranes from single pore scale to high density multipore membranes. The control of pore number, their shape and their surface properties allows many applications such as biosensing[32–36], stimulus responsive ionic channels[37–40], energy harvesting[41] and so on. To involve high charge density, the functionalization with polyelectrolytes seems a good solution regarding previous study[23,41]. However another option could be more efficient. Recently by learning from electric-eel, M.

Mayer's group obtain an open-circuit potential differences of over 100 V by stacking thousands of highly charged and salinity-containing hydrogel cells[42]. But limited by the current density, the power density at 27 mW m^{-2} can be improvable. Following this work, we synthesize in-situ a cation-selective gel using 3-sulfopropyl acrylate and an anion-selective gel using (3-acrylamidopropyl)trimethylammonium directly inside nanopore. Due to the high densities of sulfonic and quaternary ammonium groups, we assume that these hydrogels will involve a high concentration of counter-ions inside the nanopore generating a high ionic selectivity. On the same time, we consider two nanopore geometries: conical and cylindrical. As the conical pore has ionic diode propertied, we expect that the ionic selectivity will be enhanced; meanwhile this shape limits the membrane at low pore density due to the large diameter of base side. Conversely, the cylindrical pore does not have a broken symmetry and thus the performance could be lower, but it can be scaled up to a high pore density.

So our investigation will begin with conical and cylindrical single nanopores filled with hydrogels. Through these nanopores the ionic transport properties, ionic selectivity and energy conversion ability are studied. Then hydrogel functionalized conical and cylindrical multipore membranes are studied to evaluate the power generation. Finally, the power density is measured on a stacked of membranes. A clear relationship between single nanopore and a stack of high density membranes is shown.

2. Materials and methods

2.1. Materials

13 μm thick PET films, with biaxial orientations were purchased from Goodfellow (ref ES301061). 3-sulfopropyl acrylate potassium salt (SPAK) (251631), (3-acrylamidopropyl)-trimethylammonium chloride (APTAC) (448281), acrylamide (01700), 2-Hydroxy-4'-(2-

hydroxyethoxy)-2-methyl-propiophenone (photoinitiator) (410895), N,N'-Methylenebisacrylamide (BIS) (M7279), tetramethyl-ethylenediamine (TEMED) (T7024), ammonium persulfate (APS) (A3678), sodium chloride (71380) are purchased from Sigma-Aldrich. Chloride acid (20248.290) and sodium hydroxide (28245.298) are purchased from VWR Chemicals. Water used in these experiments was purified by Q-grad®-1 Milli-Q system (Millipore).

2.2. Synthesis of ion selective gels

Anionic gel: Chemicals are weighed and dissolved in water to prepare a precursor solution at 2 ml with 2.0 M 3-sulfopropyl acrylate (potassium salt), 0.045 M photoinitiator, 1.9 M acrylamide and 0.055 M BIS. For the experiments with different amounts of BIS to compare the effect of different gel reticulation degrees, three concentrations of BIS are used as R_3 = 0.055 M, R_2 = 0.037 M and R_1 = 0.018 M. Then 0.005 M APS and 0.033 M TEMED were added to the solutions as catalyst. Very quickly the nanopore membrane is immerged into the solution and make sure that both sides of membrane are well infiltrated. The solution is well isolated from air and the reaction is during overnight. Cationic gel: The same procedure is applied with a different precursor solution with 2.0 M (3-acrylamidopropyl)trimethylammonium chloride, 2.75 M acrylamide and 0.034 M BIS.

2.3. Track-etched nanopores

Single nanopores and multipore membranes were obtained by track-etched methods. The tracks were produced by Xe irradiation (8.98 MeV u^{-1}) in PET film at GANIL, SME line (Caen, France). For single track, a hole (diameter 1 mm) with a shutter was placed on ion beam path. The control of track number was provided by a detector placed behind the sample. For multipore membrane the beam directly irradiates the sample. For conical single and multipore membrane,

after being activated by UV irradiation (Fisher bioblock; VL215.MC, l= 312 nm) during 9 hours for the tip side and 15 hours for the base side, the PET film was mounted in a Teflon cell with two chambers. An etchant solution (9 M NaOH) and a stopping solution (1 M KCl and 1 M acetic acid) were used for each side to have an asymmetrical conical shape. A reference was placed in the stopping solution and a working electrode the etchant solution. A potential 1 V was applied across the film to control the pore opening by measuring the current as a function of time using an amplifier (HEKA EPC10). Then the etching process was stopped by replacing the etchant solution with stopping solution and finally the membrane was immerged in 18.2 MΩ cm pure water for 24 hours.

For cylindrical single and multipore, the same UV treatment was performed then the PET film was immerged in an etchant solution (3 M NaOH) at 50°C during 10 minutes to obtain a pore diameter about 100 nm. Finally, the membrane was also let in 18.2 MΩ cm pure water for the next use.

The diameter of single nanopore is calculated from the dependence of the conductance G measured in the linear zone of the I–V curve (-60mV to 60mV) in 1 M NaCl solution.

$$G = \frac{\kappa d D \pi}{4L} \quad (1)$$

where, κ is the ionic conductivity of the solution assuming a bulk like transport, L is the nanopore length (13 μm). For cylindrical nanopore $d = D$, meanwhile, for conical nanopore d and D are the tip and base diameter respectively. D is calculated from the total etching time t using the relationship $D = 2.5\ t$ (the factor 2.5 is determined in our experimental set up using multipore track-etched membranes).

2.4. Current-voltage measurement

Current-voltage measurements for single nanopore were performed using a patch-clamp amplifier (EPC10 HEKA electronics, Germany) with Ag/AgCl, 1 M KCl electrodes. As shown in figure S2 the pore is in the same Teflon cell of etching procedure. The two chambers of the cell were filled with the same electrolyte solution for the symmetric measurements. For asymmetric measurements, the cis side (ground electrode) had the same concentration while the concentration varied on the trans side (working electrode). For conical nanopore, tip side is always with cis side. Current traces were recorded as a function of time from 1 V to -1 V by steps of 100 mV during 2 s each and from 100 mV to -100 mV by steps of 10 mV during 2 s each.

The current and voltage measurement for multipore membrane were performed by an electrometer (Kethley 610) and a multimeter (Agilent 34410A) with Ag/AgCl electrodes. The unitary membrane is measured in the same Teflon cell as single pore while stacked membranes are mounted in a Plexiglas cell. The solution flow is driven by peristaltic pump mimipuls 3 (Gilson)

3. Results and discussions:

3.1. Single nanopore design and characterization

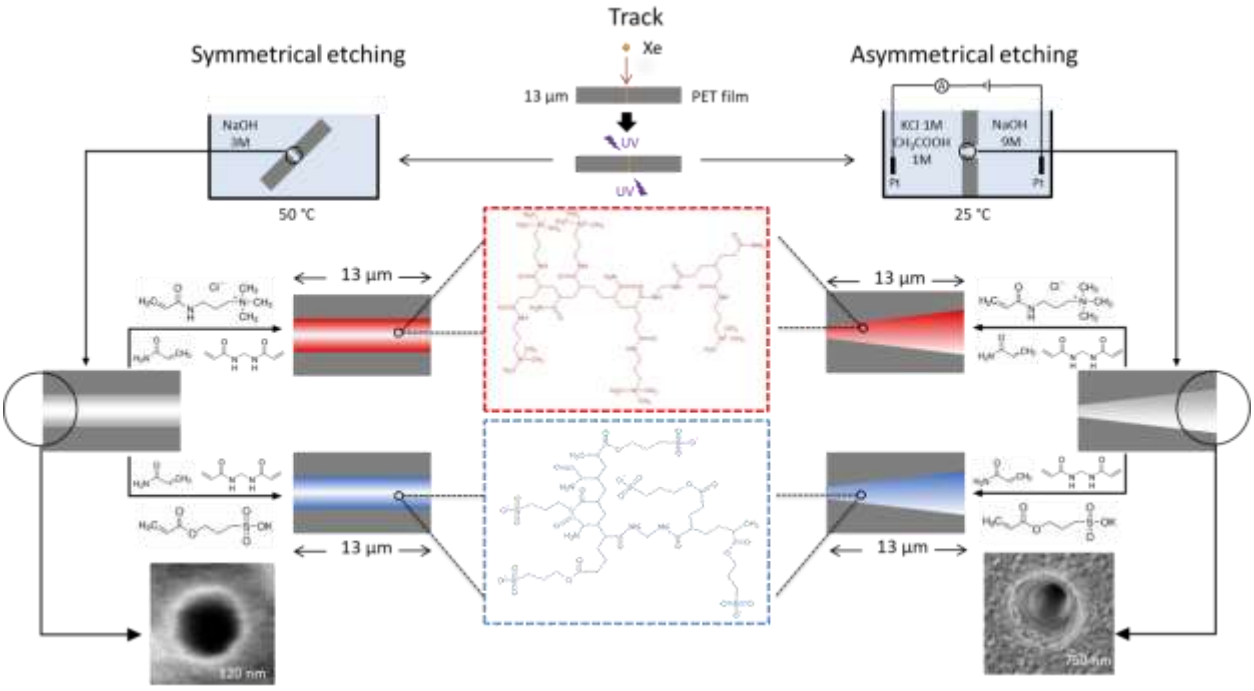

Figure 1. Schematic representation of cylindrical and conical track-etched nanoporefabrication and functionalization by polyacrylamide hydrogels.

For nanopore functionalization with anionic or cationic polyacrylamide hydrogel, the gelation procedure inside the pore was carried out by adding the precursor solution and catalyst directly at both sides of nanopores. As showed in figure 1, for cationic hydrogel, a quaternary ammonium containing molecule APTAC is polymerized with acrylamide and cross-linked with BIS, while for anionic hydrogel, a sulfonic acid terminated molecule SPAK is used for negative charges. The reactions were let during whole night well protected from air which can destroy the polymerization.

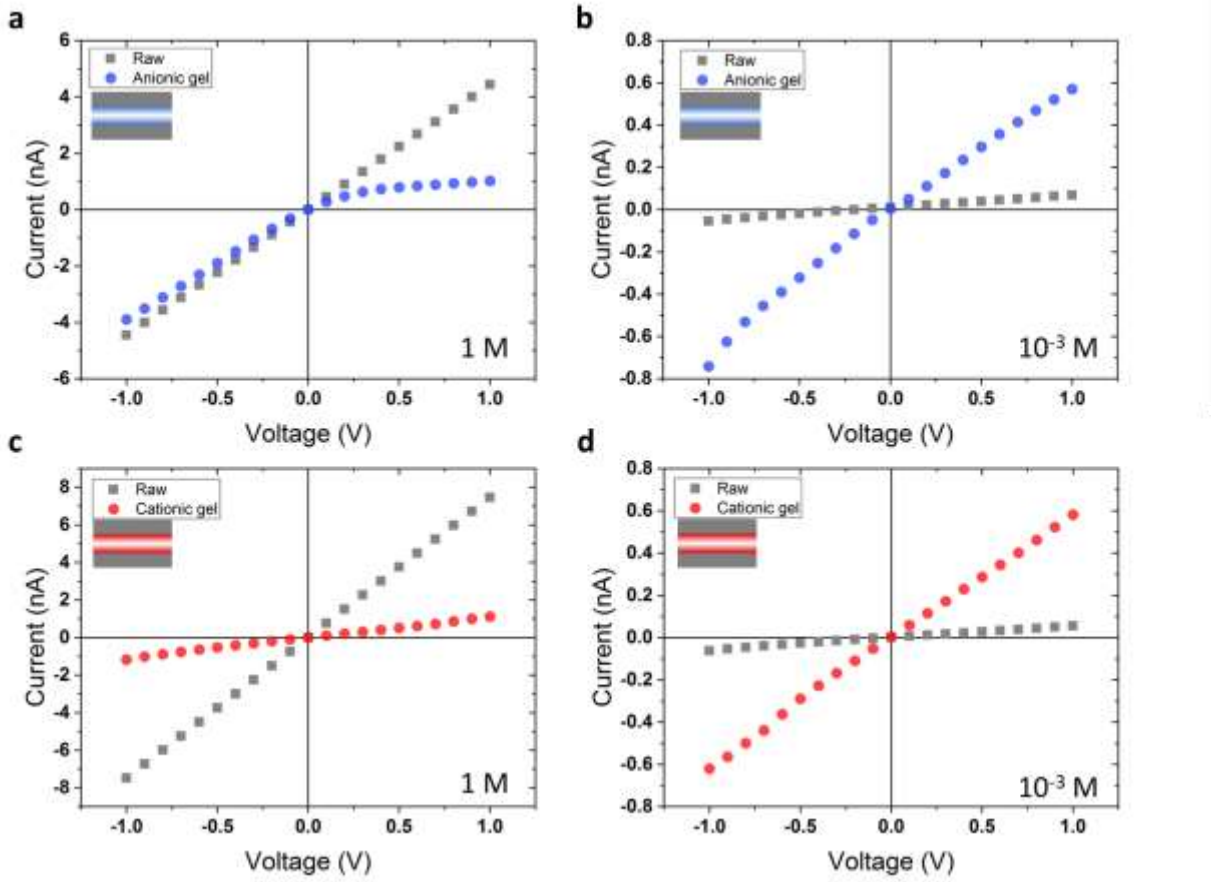

Figure 2. I-V curves of single cylindrical nanopore (diameter D = 92 nm) before (raw) and after being filled by anionic polyacrylamide hydrogel (a) measured in 1M NaCl solution pH 7.0 (b) measured in 10^{-3} M NaCl solution pH 7.0. I-V curves of single cylindrical nanopore (diameter *D* = 101 nm) before (raw) and after being filled by cationic polyacrylamide hydrogel (c) measured in 1M NaCl solution pH 7.0 (d) measured in 10^{-3} M NaCl solution pH 7.0.

First of all, we have to prove that our protocol to synthetize the gel inside the nanopore works. To do so, current−voltage (I−V) measurements were performed before and after filling gels to show the changes of ionic transport properties for each single nanopore. For cylindrical nanopores, the experiments were first performed with NaCl solution at high concentration (1 M). After gel addition, the I-V curve (figure 2, a and c) show a decrease of slope which means a

decrease of electrical conductance. In the case of nanopore with a diameter about 100 nm at 1 M of NaCl, the Debye distance is negligible. Thus the conductance can be assimilating to the bulk solution. So the decrease of conductance can be assigned to a reduction of the pore volume which is occupied by polymer chain of the gel. For the pore with anionic gel (figure 2 a), additionally to a decrease of conductance, we observe a rectification lower than 1 which means that the nanopore is selective to cation as conical one. Conversely to 1 M, the I-V curve slope measured at low NaCl concentration (10^{-3} M) increase a lot after filling with gel. This can be assigned to the presence of a large amount of counter-ions inside the pore which shield the polymer charge, these evidences confirm that the pores is filled with gel functions.

For conical nanopore (figure S1), the rectification is observed for both two gel functionalized nanopore at high concentration as shown in figure S1. The pore with anionic gel is selective to cations with a rectification factor ($R_f = |I_{+1V}/I_{-1V}|$) smaller than 1. On the contrary the cationic gel is selective to anion and thus the R_f higher than 1. In dilute solution, cationic gel conical pore has always a high rectification because of the highly charged gel at the entrance of the tip side and anionic pore shows a high conductance which confirms the large amount of counter-ions for another time.

3.2. Ionic transport properties

To better investigate the effect of gel on the nanopore charges, we investigate the conductance for a series of NaCl concentration from 10^{-4} M to 1 M (figure 3). For functionalized nanopores with anionic and cationic gel, we can find a cross between conductance-concentration curves before and after gel addition. At low salt concentration the counter ions that ensure the nanopore electroneutrality drive the conductance. With the increase of salt concentration the steric effect

becomes dominant and the conductance with gel is lower than the one without gel. For the positive charged pore, the ionic conductance slightly changes from 10^{-4} M to 1 M compared with the pore without gel. This suggests that the gel makes the nanopore highly charged due to a dense framework. In this case, the ionic transport is strongly dominated by counter ions rather than bulk solution. For anionic pore, we synthesized the gels with different amounts of crosslinker ($R_3 > R_2 > R_1$). We can observe at low salt concentration a higher conductance with the increase of crosslink degree (figure 3, b). In this case, the gel becomes denser increasing the concentration of counter ion. For the conical nanopore (figure S2), cationic gel has the same effect as in cylindrical one. The ionic conductance raises a lot at low salt concentration with the presence of charges and decrease at high concentration due to the steric effect.

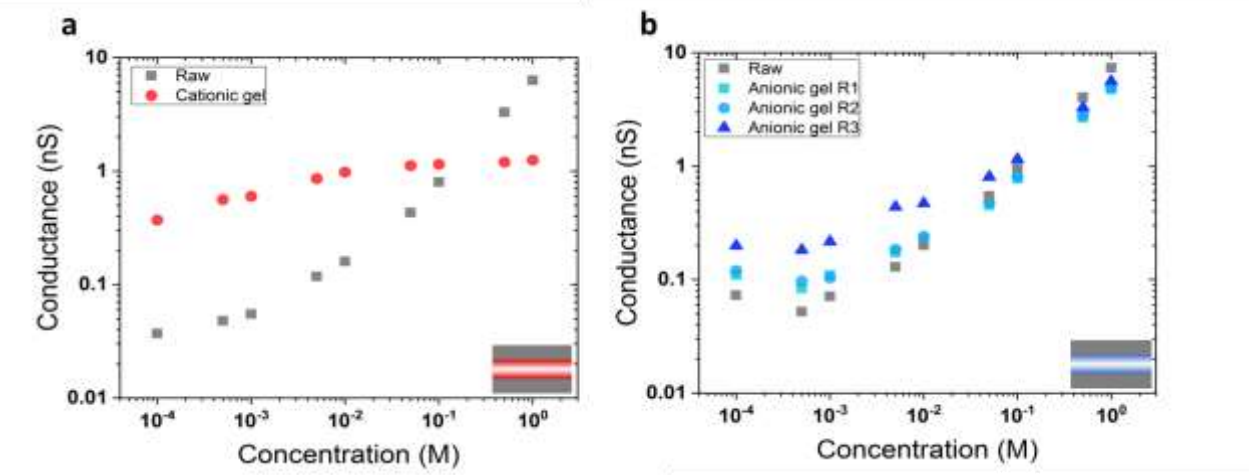

Figure 3. Conductance of cylindrical nanopore (a) with cationic gel (D = 101 nm) and (b) with anionic gel (BIS concentration $R_3 > R_2 > R_1$) according to salt concentration (D_{R1} = 95 nm, D_{R2} = 92 nm, D_{R3} = 92 nm.)

With the high charge density inside the pore and a conductivity driven by the counter ion, the nanopore should be highly selective especially with the conical shape. The first indication of that

comes from the property of ionic current rectification characterized by the rectification factor (R_f). Figure 4 shows the rectification factors varying with NaCl concentrations for cylindrical and conical pores filled with cationic and anionic gel. For the cylindrical pore filled with cationic gel (figure 4, a), the R_f closed to 1 regardless of the electrolytes concentration with and without gel. This means that even if the gel charges governed ionic transport regime, ionic accumulation and depletion do not occurs inside the membrane. On the contrary, the anionic gel induces an ionic current rectification. The R_f lower than 1 between 10^{-3} M and 1 M show a selectivity to cation that is consistent with the negative charge of the gel. We observe also that with a higher crosslink degree R_f value decrease. This means that when the gel is more dense and thus the nanopore more charged the ionic rectification factor is closer than 1. This agrees the behavior observe for the nanopore functionalized with cationic gel. The origin of current rectification is not well elucidated. However one assumption can be expressed. An inhomogeneity of gel distribution along the nanopore could create some ion depletion zone inducing rectification behavior.

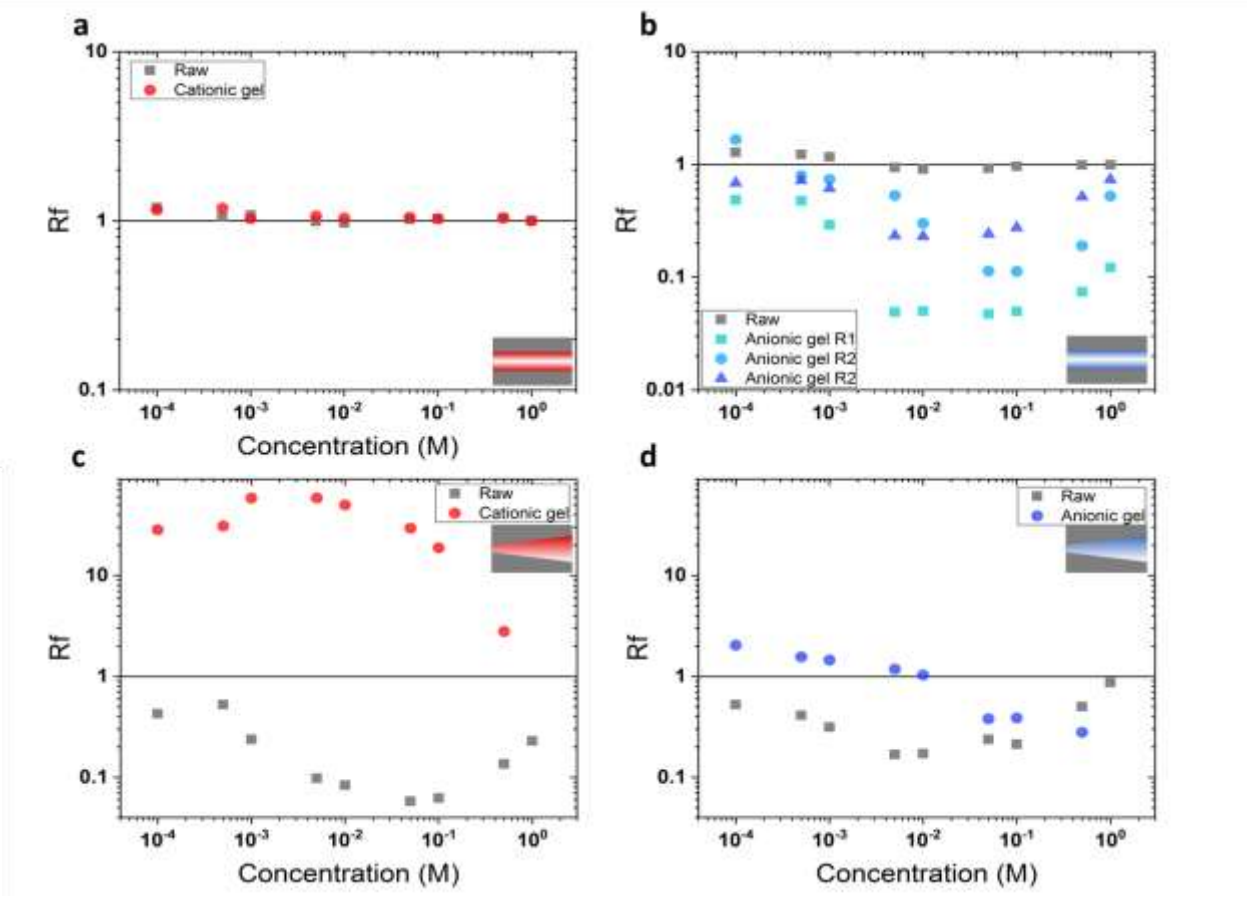

Figure 4. Rectification of cylindrical nanopore with (a) cationic gel (D = 101 nm) (b) anionic gel (D_{R1} = 95 nm, D_{R2} = 92 nm, D_{R3} = 92 nm.), of conical nanopore with (c) cationic gel (d = 79 nm, D = 497 nm) (d) anionic (d = 70 nm, D = 412 nm) gel in terms of salt concentration, with C_{max}/C_{min} = 1000.

For the conical nanopore, a very distinct R_f change is observed after functionalization with cationic gel (figure 4, c). With the conical geometry, ionic depletion occurs near the positive charge dominated membrane which involves high selectivity to anion. While with anionic gel, rectification behavior takes place only at high concentration selective to cations. At low concentration, a high ionic conductance reduces impact of the ionic accumulation and ionic depletion, thus the rectification becomes negligible.

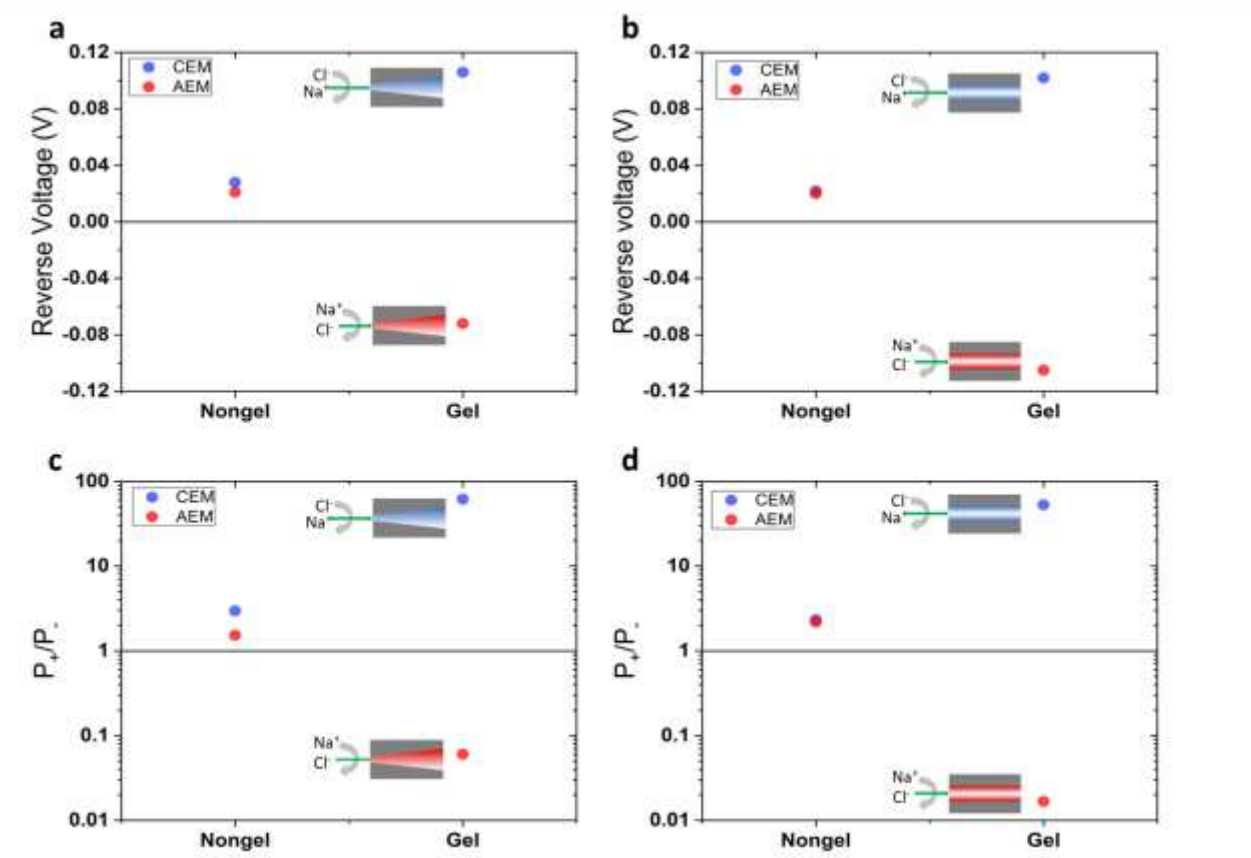

Figure 5. Reverse voltage generated by gel functionalization in (a) conical nanopore (b) cylindrical nanopore and ionic selectivity corresponding in (c) conical nanopore (d) cylindrical nanopore, with C_{max}/C_{min} = 1000. Cylindrical pore $D_{anionic}$ = 92 nm, $D_{cationic}$ = 101 nm, conical anionic d = 70 nm, D = 412 nm and conical cationic d = 79 nm, D = 497 nm.

The nanopore selectivity can be directly obtained from the reverse voltage under transmembrane concentration gradient. To do so a NaCl solution of 1 M at pH 7.0 and a NaCl solution of 10^{-3} M at pH 7.0 are added in each side of the cell, for cylindrical nanopores. For conical nanopores, the high concentration is placed on the tip side; and the low one to the base side. From the I-V curves, we can directly get the intercepts on the current and voltage axes which present short-circuit current (I_{SC}) and open-circuit voltage (V_{OC}). The V_{OC} has two contributions: one is from

the osmotic diffusion effect and the other one is from redox Nernst potential on the electrodes. For all results showed here, this second term is subtracted by using $V_{rev} = V_{oc} - E_{redox}$.

Figure 5, a and b show the reversal voltage measured for nanopore filled with gels. From this value, we calculate the corresponding ionic selectivity calculated via the Goldman–Hodgkin–Katz voltage equation[43]:

$$V_{rev} = \frac{k_B T}{e} \ln\left(\frac{P_{Na^+}/P_{Cl^-} \times C_{high} + C_{low}}{P_{Na^+}/P_{Cl^-} \times C_{low} + C_{high}}\right) \quad (2)$$

where P_{Na^+}/P_{Cl^-} is the selectivity, C_{high} and C_{low} are the electrolytes concentrations, k_B is the Boltzmann constant, T is the solution temperature and e is the electron charge.

As the non-functionalized PET nanopore has –COOH groups on the inner surface wall, at pH 7.0 the surface has negative charged. This gives to the nanopore a cationic selectivity confirmed by the reversal voltage at around 0.02 – 0.03 V. After filling with anionic hydrogels, the nanopore charges increase, so a significant higher reverse voltage is obtained up to 0.10 V which also present a cation selectivity about 50-70. Meanwhile, with cationic gel, the nanopore gets inversed selectivity characterized by a negative reversal voltage. In this case the anions can be much easier to pass through the nanopore). It is interesting to notice that the ratios P_{Na^+}/P_{Cl^-} are close for the conical and the cylindrical nanopore. This result was totally unexpected, however, it is relatively consistent with the fact that the ionic transport though the nanopore is governed by the gel. In this case, the effect of geometry on the conductance and the selectivity seem shield.

3.3. Energy generated from single nanopore

The energy conversion performance is also investigated by applying a transmembrane concentration gradient under salinity gradient of C_{max}/C_{min} = 1000.

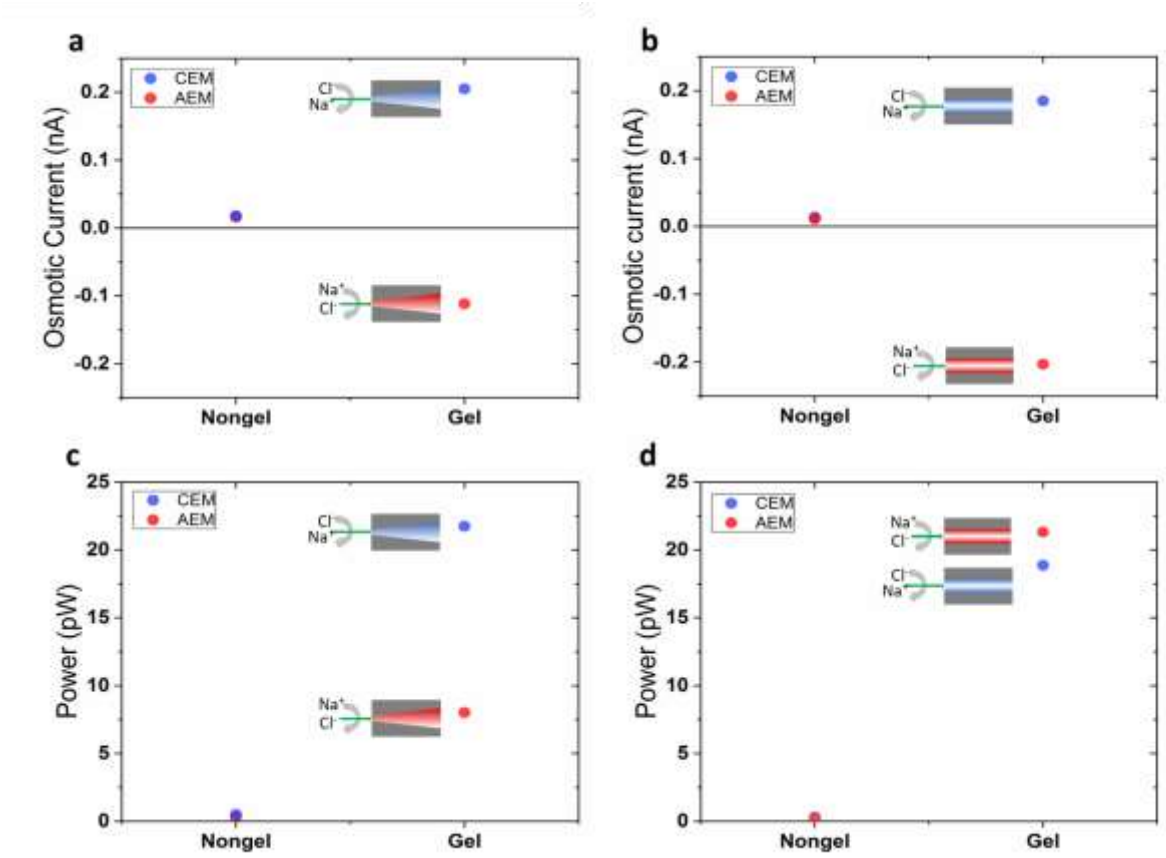

Figure 6. Osmotic current generated by gel functionalization in (a) conical nanopore (b) cylindrical nanopore, and single pore power corresponding in (c) conical nanopore (d) cylindrical nanopore. C_{max}/C_{min} = 1000. Cylindrical pore $D_{anionic}$ = 92 nm, $D_{cationic}$ = 101 nm, conical anionic d = 70 nm, D = 412 nm and conical cationic d = 89 nm, D =497 nm.

The osmotic currents (I_{oms}) are calculated using $I_{osm}=I_{mes} - G\times E_{redox}$, where I_{mes} is the intercepts on the current axes which present short-circuit current (I_{SC}).Like reversal potentials, the raw PET pore has a small osmotic current due to the presence of –COO- groups at pH 7.0 (figure 6). After

filling with gel, we observe a huge increase of osmotic current from about 10 pA up to about +/- 200 pA. Together with the reversal potential, we calculate the power generated with a single nanopore. The single pore power is obtained at around 20 pW regardless of the pore shape or gel charge. It is competitive compared with other single nanopores such as boron nitride nanotube (20 pW)[17] and monolayer molybdenum disulfide (500 pW)[18].

3.4 Energy generated from multipore membranes and membranes stacks

To go further on harvesting of osmotic energy, the gel inclusion process was implemented on multipore membranes (Figure 7). First, the experiments were carried out on membranes with low pore density (5.10^5 pores cm^{-2}). The same track-etching procedure is adopted for multipore membrane fabrication. The membrane thickness is always 13 µm . Two geometries are tested to compare their performance. Cylindrical membrane has a pore size of 156 nm ± 22 nm and 172 nm ± 29 nm for each side while conical nanopore has a pore size of 753 nm ± 42 nm for base side and 77 nm ± 11 nm for tip side. The transmembrane voltage under per multipore membrane equals to 0.1 V as the same of the single nanopore. The membrane surface measured here is 0.28 cm2. For anionic cylindrical and conical membranes, the current density is measured as 0.29 A m^{-2} and 0.23 A m^{-2}. Multiplied by voltage, we get a power density as 0.03 W m^{-2} and 0.02 W m^{-2}. If we calculate the theoretical power density based on the values of single nanopore (20 pW $pore^{-1}$), we can get it as 0.1 W m^{-2}. It has an obvious loss on power density for multipore membrane.

With stack of four membranes the transmembrane voltage generated by the difference of salinity are summed to reach about 0.4 V. Another time we get quite similar results between cylindrical and conical pores as cylindrical membranes get 0.41 V and 0.86 µA while conical membranes

get 0.81 µA. This result confirms again that the ionic transport is governed by gel charges rather than the nanopore geometry. According to that the cylindrical pore can be used as conical one to generate osmotic current. The interest of cylindrical pore is the possibility to fabricate membranes with higher pore densities. By using the membrane surface as 0.28 cm^2 of each cell, the power density is calculated as 0.01 W m^{-2}. By stacking membranes, global power density decreases almost two third because of the high resistance which comes from the long distance between two cells and the low concentration at 10^{-3} M.

The same procedure was used to design membrane with a pore density of 3.10^9 cm^{-2} of cylindrical nanopore. By stacking 4 membranes, the voltage stays at 0.39 V and the current reach at 107 µA so the total power is obtained as 37.7 µW (each membrane surface 0.28 cm^2). The power density is calculated as 0.37 W m^{-2}. From 2.10^5 to 3.10^9 the pore density becomes 15000 times larger while the current increases only 51 times. With this high pore density, the tracks can be crossed and the pore shapes can be non-regular, so when the pore density becomes large enough, there will not be a linear relation between the pore density and the current density. However this can be improved using a low fluency coupled with a large number of ion beam passage to perform track. In addition, one limit of our stack is the distance inter-membrane of 1 cm that involves a very large resistance decreasing the performance.

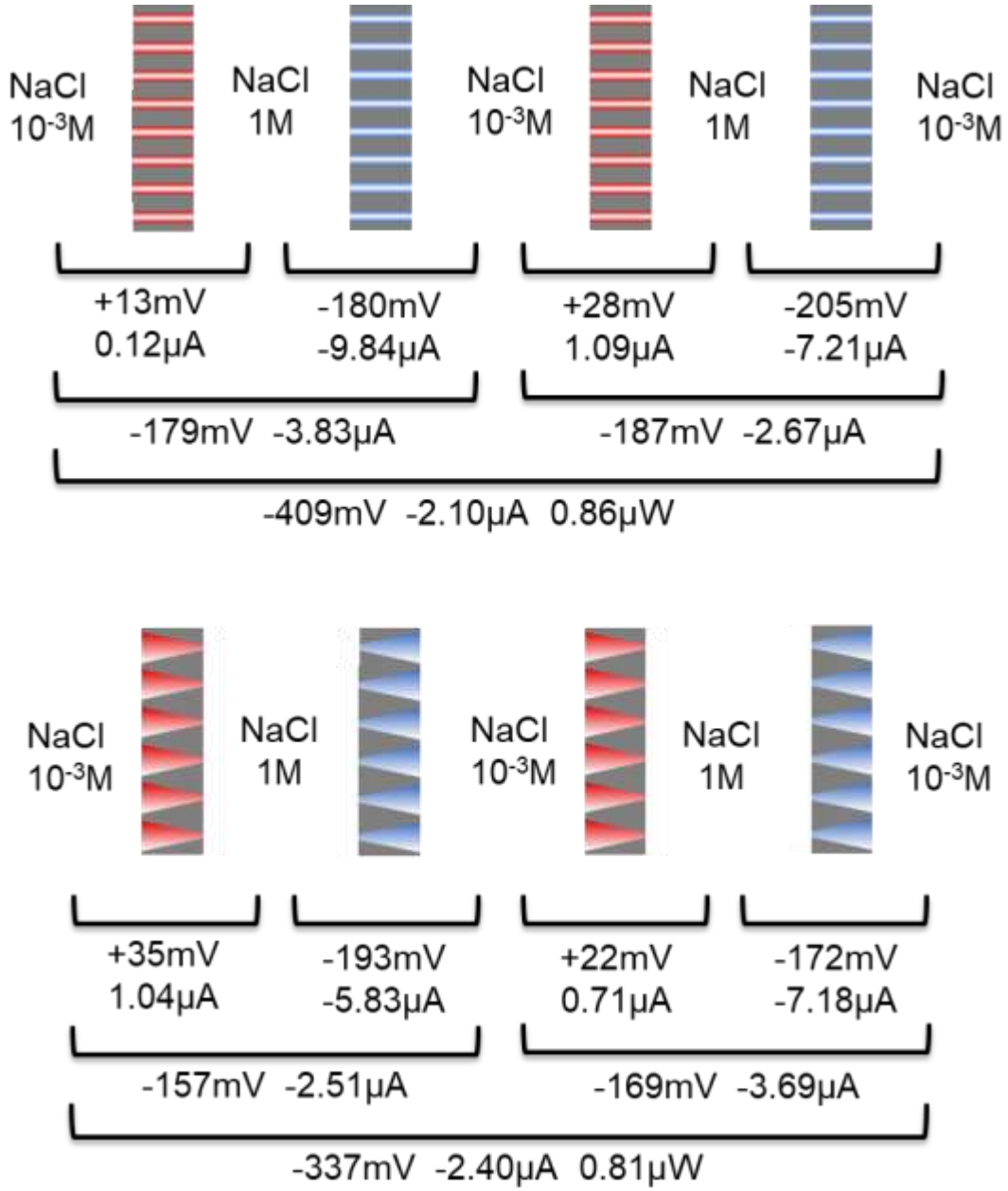

Figure 7. Voltage and current measured across the functionalized multipore membranes with a pore density of 2.10^5 cm^{-2}. Membrane thickness = 13µm.

4. Conclusions

In summary, in this work we demonstrate the use of a track etched polymer nanopore membrane for harvesting the osmotic energy. The nanopores were functionalized by filling with highly

charged hydrogels. The ionic transport properties investigate at single nanopore scale show that it is governed essentially by the gel charge shielding the effect of geometry. Because the performance of energy conversion is almost independent of the nanopore shape, the cylindrical geometry is proved as a good candidate for high pore density membranes. The functionalized nanopores show high ionic selectivity and good energy conversion ability with a power density of about 0.37 W m^{-2} working in pH 7. By improving the direction of tracks and the inter membrane distances we could improve the energy yield and thus consider such membrane for real application.

Supporting Information:

Additional informations (S1 – S5) (PDF) are available in supporting information.

Acknowledgement:

Single tracks have been produced in GANIL (Caen, France) in the framework of an EMIR project.

Corresponding Author

E-mail: sebastien.balme@umontpellier.fr. Tel: (33) 4 67 14 91 18.

References:

(1) Chu, S.; Majumdar, A. Opportunities and Challenges for a Sustainable Energy Future. *Nature* **2012**, *488* (7411), 294–303. https://doi.org/10.1038/nature11475.

(2) Stocker, T. F.; Qin, D.; Plattner, G. K.; Tignor, M. M. B.; Allen, S. K.; Boschung, J.; Nauels, A.; Xia, Y.; Bex, V.; Midgley, P. M. *Climate Change 2013 the Physical Science Basis: Working Group I Contribution to the Fifth Assessment Report of the*

Intergovernmental Panel on Climate Change; 2013; Vol. 9781107057. https://doi.org/10.1017/CBO9781107415324.

(3) Roemmich, D.; Church, J.; Gilson, J.; Monselesan, D.; Sutton, P.; Wijffels, S. Unabated Planetary Warming and Its Ocean Structure since 2006. *Nat. Clim. Chang.* **2015**, *5* (3), 240–245. https://doi.org/10.1038/nclimate2513.

(4) Fargione, J.; Hill, J.; Tilman, D.; Polasky, S.; Hawthorne, P. Land Clearing and the Biofuel Carbon Debt. *Science.* **2008**, *319*(5867), 1235-1238. https://doi.org/10.1126/science.1152747.

(5) Lewis, N. S. Research Opportunities to Advance Solar Energy Utilization. *Science*. 2016, *351*(6271), aad1920. https://doi.org/10.1126/science.aad1920.

(6) Joselin Herbert, G. M.; Iniyan, S.; Sreevalsan, E.; Rajapandian, S. A Review of Wind Energy Technologies. *Renewable and Sustainable Energy Reviews*. 2007, *11*(6), 1117-1145. https://doi.org/10.1016/j.rser.2005.08.004.

(7) Bertani, R. Geothermal Power Generation in the World 2010-2014 Update Report. *Geothermics* **2016**, *60*, 31-43. https://doi.org/10.1016/j.geothermics.2015.11.003.

(8) Logan, B. E.; Elimelech, M. Membrane-Based Processes for Sustainable Power Generation Using Water. *Nature*. 2012, *488*(7411), 313-319. https://doi.org/10.1038/nature11477.

(9) Siria, A.; Bocquet, M. L.; Bocquet, L. New Avenues for the Large-Scale Harvesting of Blue Energy. *Nat. Rev. Chem.* **2017**, *1* (11), 0091. https://doi.org/10.1038/s41570-017-0091.

(10) Ramon, G. Z.; Feinberg, B. J.; Hoek, E. M. V. Membrane-Based Production of Salinity-Gradient Power. *Energy and Environmental Science*. **2011**, *4*(11), 4423-4434. https://doi.org/10.1039/c1ee01913a.

(11) Post, J. W.; Veerman, J.; Hamelers, H. V. M.; Euverink, G. J. W.; Metz, S. J.; Nymeijer, K.; Buisman, C. J. N. Salinity-Gradient Power: Evaluation of Pressure-Retarded Osmosis and Reverse Electrodialysis. *J. Memb. Sci.* **2007**, *288*(1-2), 218-230. https://doi.org/10.1016/j.memsci.2006.11.018.

(12) She, Q.; Jin, X.; Tang, C. Y. Osmotic Power Production from Salinity Gradient Resource by Pressure Retarded Osmosis: Effects of Operating Conditions and Reverse Solute Diffusion. *J. Memb. Sci.* **2012**, 401-402, 262-273. https://doi.org/10.1016/j.memsci.2012.02.014.

(13) Achilli, A.; Cath, T. Y.; Childress, A. E. Power Generation with Pressure Retarded Osmosis: An Experimental and Theoretical Investigation. *J. Memb. Sci.* **2009**, *343*(1-2), 42-52. https://doi.org/10.1016/j.memsci.2009.07.006.

(14) Post, J. W.; Hamelers, H. V. M.; Buisman, C. J. N. Energy Recovery from Controlled Mixing Salt and Fresh Water with a Reverse Electrodialysis System. *Environ. Sci. Technol.* **2008**, *42*(15), 5785-5790. https://doi.org/10.1021/es8004317.

(15) Tedesco, M.; Cipollina, A.; Tamburini, A.; Micale, G. Towards 1 KW Power Production in a Reverse Electrodialysis Pilot Plant with Saline Waters and Concentrated Brines. *J. Memb. Sci.* **2017**, *522*, 226-236. https://doi.org/10.1016/j.memsci.2016.09.015.

(16) Veerman, J.; Saakes, M.; Metz, S. J.; Harmsen, G. J. Electrical Power from Sea and River Water by Reverse Electrodialysis: A First Step from the Laboratory to a Real Power Plant. *Environ. Sci. Technol.* **2010**, *44* (23), 9207–9212. https://doi.org/10.1021/es1009345.

(17) Siria, A.; Poncharal, P.; Biance, A. L.; Fulcrand, R.; Blase, X.; Purcell, S. T.; Bocquet, L. Giant Osmotic Energy Conversion Measured in a Single Transmembrane Boron Nitride Nanotube. *Nature* **2013**, *494* (7438), 455–458. https://doi.org/10.1038/nature11876.

(18) Feng, J.; Graf, M.; Liu, K.; Ovchinnikov, D.; Dumcenco, D.; Heiranian, M.; Nandigana, V.; Aluru, N. R.; Kis, A.; Radenovic, A. Single-Layer MoS2nanopores as Nanopower Generators. *Nature* **2016**, *536* (7615), 197–200. https://doi.org/10.1038/nature18593.

(19) Ji, J.; Kang, Q.; Zhou, Y.; Feng, Y.; Chen, X.; Yuan, J.; Guo, W.; Wei, Y.; Jiang, L. Osmotic Power Generation with Positively and Negatively Charged 2D Nanofluidic Membrane Pairs. *Adv. Funct. Mater.* **2017**, *27* (2), 201603623. https://doi.org/10.1002/adfm.201603623.

(20) Secchi, E.; Marbach, S.; Niguès, A.; Stein, D.; Siria, A.; Bocquet, L. Massive Radius-Dependent Flow Slippage in Carbon Nanotubes. *Nature* **2016**, *537* (7619), 210-213. https://doi.org/10.1038/nature19315.

(21) Vlassiouk, I.; Siwy, Z. S. Nanofluidic Diode. *Nano Lett.* **2007**, *7* (3), 552–556. https://doi.org/10.1021/nl062924b.

(22) Siwy, Z. S. Ion-Current Rectification in Nanopores and Nanotubes with Broken Symmetry. *Adv. Funct. Mater.* **2006**, *16* (6), 735–746. https://doi.org/10.1002/adfm.200500471.

(23) Ma, T.; Gaigalas, P.; Lepoitevin, M.; Plikusiene, I.; Bechelany, M.; Janot, J. M.; Balanzat, E.; Balme, S. Impact of Polyelectrolyte Multilayers on the Ionic Current Rectification of Conical Nanopores. *Langmuir* **2018**, *34* (11), 3405–3412. https://doi.org/10.1021/acs.langmuir.8b00222.

(24) Gao, J.; Guo, W.; Feng, D.; Wang, H.; Zhao, D.; Jiang, L. High-Performance Ionic Diode Membrane for Salinity Gradient Power Generation. *J. Am. Chem. Soc.* **2014**, *136* (35), 12265–12272. https://doi.org/10.1021/ja503692z.

(25) Zhang, Z.; Sui, X.; Li, P.; Xie, G.; Kong, X. Y.; Xiao, K.; Gao, L.; Wen, L.; Jiang, L. Ultrathin and Ion-Selective Janus Membranes for High-Performance Osmotic Energy Conversion. *J. Am. Chem. Soc.* **2017**, *139* (26), 8905–8914. https://doi.org/10.1021/jacs.7b02794.

(26) Zhang, Z.; Kong, X. Y.; Xiao, K.; Liu, Q.; Xie, G.; Li, P.; Ma, J.; Tian, Y.; Wen, L.; Jiang, L. Engineered Asymmetric Heterogeneous Membrane: A Concentration-Gradient-Driven Energy Harvesting Device. *J. Am. Chem. Soc.* **2015**, *137* (46), 14765–14772. https://doi.org/10.1021/jacs.5b09918.

(27) Lepoitevin, M.; Ma, T.; Bechelany, M.; Janot, J. M.; Balme, S. Functionalization of Single Solid State Nanopores to Mimic Biological Ion Channels: A Review. *Advances in Colloid and Interface Science*. **2017**, pp 195–213. https://doi.org/10.1016/j.cis.2017.09.001.

(28) Ali, M.; Schiedt, B.; Healy, K.; Neumann, R.; Ensinger, W. Modifying the Surface Charge of Single Track-Etched Conical Nanopores in Polyimide. *Nanotechnology* **2008**, *19* (8). https://doi.org/10.1088/0957-4484/19/8/085713.

(29) Apel, P. Y.; Ramirez, P.; Blonskaya, I. V.; Orelovitch, O. L.; Sartowska, B. A. Accurate Characterization of Single Track-Etched, Conical Nanopores. *Phys. Chem. Chem. Phys.* **2014**, *16* (29), 15214–15223. https://doi.org/10.1039/c4cp01686f.

(30) Siwy, Z.; Apel, P.; Dobrev, D.; Neumann, R.; Spohr, R.; Trautmann, C.; Voss, K. Ion Transport through Asymmetric Nanopores Prepared by Ion Track Etching. In *Nuclear Instruments and Methods in Physics Research, Section B: Beam Interactions with*

Materials and Atoms; **2003**, *208*, 143–148. https://doi.org/10.1016/S0168-583X(03)00884-X.

(31) Siwy, Z.; Fuliński, A. Fabrication of a Synthetic Nanopore Ion Pump. *Phys. Rev. Lett.* **2002**, *89* (19), 198103. https://doi.org/10.1103/PhysRevLett.89.198103.

(32) Giamblanco, N.; Coglitore, D.; Gubbiotti, A.; Ma, T.; Balanzat, E.; Janot, J. M.; Chinappi, M.; Balme, S. Amyloid Growth, Inhibition, and Real-Time Enzymatic Degradation Revealed with Single Conical Nanopore. *Anal. Chem.* **2018**, *90*, 12900–12908. https://doi.org/10.1021/acs.analchem.8b03523.

(33) Lepoitevin, M.; Jamilloux, B.; Bechelany, M.; Balanzat, E.; Janot, J. M.; Balme, S. Fast and Reversible Functionalization of a Single Nanopore Based on Layer-by-Layer Polyelectrolyte Self-Assembly for Tuning Current Rectification and Designing Sensors. *RSC Adv.* **2016**, *6* (38), 32228–32233. https://doi.org/10.1039/c6ra03698h.

(34) Lepoitevin, M.; Nguyen, G.; Bechelany, M.; Balanzat, E.; Janot, J. M.; Balme, S. Combining a Sensor and a PH-Gated Nanopore Based on an Avidin-Biotin System. *Chem. Commun.* **2015**, *51* (27), 5994–5997. https://doi.org/10.1039/c4cc10087e.

(35) Hou, X.; Yang, F.; Li, L.; Song, Y.; Jiang, L.; Zhu, D. A Biomimetic Asymmetric Responsive Single Nanochannel. *J. Am. Chem. Soc.* **2010**, *132* (33), 11736–11742. https://doi.org/10.1021/ja1045082.

(36) Cabello-Aguilar, S.; Balme, S.; Chaaya, A. A.; Bechelany, M.; Balanzat, E.; Janot, J. M.; Pochat-Bohatier, C.; Miele, P.; Dejardin, P. Slow Translocation of Polynucleotides and Their Discrimination by α-Hemolysin inside a Single Track-Etched Nanopore Designed by Atomic Layer Deposition. *Nanoscale* **2013**, *5* (20), 9582–9586. https://doi.org/10.1039/c3nr03683a.

(37) Zhao, Y.; Janot, J. M.; Balanzat, E.; Balme, S. Mimicking PH-Gated Ionic Channels by Polyelectrolyte Complex Confinement Inside a Single Nanopore. *Langmuir* **2017**, *33* (14), 3484–3490. https://doi.org/10.1021/acs.langmuir.7b00377.

(38) Tomicki, F.; Krix, D.; Nienhaus, H.; Ulbricht, M. Stimuli-Responsive Track-Etched Membranes via Surface-Initiated Controlled Radical Polymerization: Influence of Grafting Density and Pore Size. *J. Memb. Sci.* **2011**, *377* (1–2), 124–133. https://doi.org/10.1016/j.memsci.2011.04.028.

(39) Zhang, Z.; Xie, G.; Xiao, K.; Kong, X. Y.; Li, P.; Tian, Y.; Wen, L.; Jiang, L. Asymmetric Multifunctional Heterogeneous Membranes for PH- and Temperature-Cooperative Smart Ion Transport Modulation. *Adv. Mater.* **2016**, *28* (43), 9613–9619. https://doi.org/10.1002/adma.201602758.

(40) Ma, T.; Walko, M.; Lepoitevin, M.; Janot, J. M.; Balanzat, E.; Kocer, A.; Balme, S. Combining Light-Gated and PH-Responsive Nanopore Based on PEG-Spiropyran Functionalization. *Adv. Mater. Interfaces* **2018**, *5* (2), 1701051. https://doi.org/10.1002/admi.201701051.

(41) Balme, S.; Ma, T.; Balanzat, E.; Janot, J. M. Large Osmotic Energy Harvesting from Functionalized Conical Nanopore Suitable for Membrane Applications. *J. Memb. Sci.* **2017**, *544*, 18–24. https://doi.org/10.1016/j.memsci.2017.09.008.

(42) Schroeder, T. B. H.; Guha, A.; Lamoureux, A.; Vanrenterghem, G.; Sept, D.; Shtein, M.; Yang, J.; Mayer, M. An Electric-Eel-Inspired Soft Power Source from Stacked Hydrogels. *Nature* **2017**, *552* (7684), 214–218. https://doi.org/10.1038/nature24670.

(43) Rollings, R. C.; Kuan, A. T.; Golovchenko, J. A. Ion Selectivity of Graphene Nanopores. *Nat. Commun.* **2016**, *7*, 11408. https://doi.org/10.1038/ncomms11408.

Table of Contents Graphic.